Nonlinear laser-induced deformations of liquid-liquid interfaces: An optical fiber model

Ole Jakob Birkeland* and Iver Brevik†
Department of Energy and Process Engineering, Norwegian University of Science and Technology, N-7491 Trondheim, Norway
(Received 15 January 2008; revised manuscript received 16 July 2008; published 24 December 2008)

Experimentally, it turns out that radiation forces from a cw laser on a liquid-liquid interface are able to produce giant deformations (up to about 100 μm), if the system is close to the critical point where the surface tension becomes small. We present a model for such a fingerlike deformation, implying that the system is described as an optical fiber. One reason for introducing such a model is that the refractive index difference in modern experiments, such as those of the Bordeaux group, is small, of the same order as in practical fibers in optics. It is natural therefore to adopt the hybrid HE_{11} mode, known from fiber theory as the fundamental mode for the liquid system. We show how the balance between hydrodynamical and radiation forces leads to a stable equilibrium point for the liquid column. Also, we calculate the narrowing of the column radius as the depth increases. Comparison with experimental results of the Bordeaux group yields quite satisfactory agreement as regards the column width.

DOI: 10.1103/PhysRevE.78.066314 PACS number(s): 47.61.−k, 42.50.Wk, 42.25.Fx

I. INTRODUCTION

Force exerted by light on continuous matter has attracted attention since the days of Maxwell. In 1869 he was the first to predict and calculate the pressure from light reflecting off a surface; in 1901 the first attempts of experimental verification were made by Lebedev, showing that the light pressure acts inward to a reflecting surface. Poynting [1] later extended the knowledge of radiation pressure by considering light incident from vacuum on the surface of a transparent dielectric, predicting the irradiation to produce an outward normal force irrespective of the angle of incidence. More recently, the experimental paper of Ashkin and Dziedzic from 1973 is a pioneering work [2]. They illumined an air-water surface by a focused pulsed laser, verifying that the force was indeed outward directed. Another recent experiment along the same lines is that of Schroll *et al.* [3].

The radiation pressure problem is related to the well-known Abraham-Minkowski controversy about the correct form of the electromagnetic energy-momentum tensor in a medium. That question has been discussed at varying degrees of intensity ever since Abraham and Minkowski presented their energy-momentum expressions around 1910. In the simplest case, when the medium is isotropic and homogeneous, the difference turns up only in the expressions for the momentum density $\mathbf{g}$: in the Minkowski case $\mathbf{g}^{\mathbf{M}}=\mathbf{D}\times\mathbf{B}$, whereas in the Abraham case, $\mathbf{g}^{\mathbf{A}}=(1/c^2)\mathbf{E}\times\mathbf{H}$, the latter expression satisfying Planck's principle of inertia of energy $\mathbf{g}=\mathbf{S}/c^2$, $\mathbf{S}$ being the Poynting vector. For an introduction to the Abraham-Minkowski problem, the reader may consult Møller's book on relativity [4], or the review article [5]. There is extensive literature in this field; some papers are Refs. [6–13]. Fortunately, for practical purposes the difference between the Abraham and Minkowski predictions goes away in optics because the influence from the "Abraham term" fluctuates out. The force can be calculated from the electromagnetic stress tensor parts only, and the stress tensors are equal in the two cases. We shall take this into account in the following, and simply call the force the Abraham-Minkowski (AM) force.

A major reason why radiation forces have attracted increased interest in recent years is their practical usefulness. In biology and medicine the need for noninvasive techniques for manipulation of individual cells or complex molecules has led to the development of optical tweezers, invented by Ashkin *et al.* in 1986 [14]. Furthermore, fluid-interface instabilities driven by the relatively strong forces from electric field [15,16] represent the cornerstone of many industrial processes such as electrospraying [17], ink-jet printing [18], and surface relief printing [19].

An important progress in the application of pressure forces is to make use of two liquids in the vicinity of the *critical point*. Then the surface tension is significantly diminished, and the effect of the pressure forces becomes enhanced. Traditionally, due to the competition with surface forces, the pressure effect has been rather minute. For instance, in the Ashkin-Dziedzic air-water pressure experiment [2], with surface tension equal to $\sigma=73$ mJ/m, the deflection of the water surface acted upon by a pulsed Nd YAG laser was only about 1 μm. Working near the critical point, the deflection can be much higher, about 50 μm or more. Moreover, in a two-fluid system of surfactant-coated nanodroplets in oil microemulsions the surface tension can be made more than 1×10^6 times smaller than the usual air-water tension (cf., for instance, Ref. [20]).

The main purpose of the present paper is to introduce a fiber model for the large finger-shaped deformations. Interesting work, both experimental and theoretical, has in recent years been done in this direction by the Bordeaux group, considering diverse effects arising from the focusing of laser beams onto a fluid-fluid interface having extremely low surface tension. Much of this work, up to 2002, is summarized in the Ph.D. thesis of Casner [21]. There are several recent papers by this group [3,22–26]. There is also a review paper [27], and related papers of others such as [28]. Whereas the first experimental and theoretical investigations dealt with small deformations in the hydrodynamic linear regime, the

*ole.jakob.birkeland@cggveritas.com
†iver.h.brevik@ntnu.no

most recent experiments have demonstrated the appearance of giant surface deformations of order 50–100 μm. Large finger-shaped structures have been observed, as well as liquid jets and shedding of microdroplets.

A theoretical description of these finger-shaped deformations is still lacking. Nor will we in the present paper attempt to give a quantitative estimate of the large deformations. Instead, we will show one can calculate a stable equilibrium radius of the liquid column. As is conventional in fiber optics, we take the HE_{11} mode to be dominant for a steplike fiber having a weak refractive index difference between core and cladding. This dominance occurs if the refractive index contrast is small, about 0.01. Actually, this fits quite well with the conditions of the Bordeaux experiments. It means that the central core becomes exposed to a laser intensity differing in shape and intensity from the conventional Gaussian intensity distribution.

There is another advantage of this kind of wave description. The radiation pressure is predicted to be nonvanishing even on the vertical walls of the cavity. The magnitude of the pressure is of the same order as the pressure from a Gaussian beam on a flat surface at normal incidence. Such a pressure is not obtainable using a ray picture of the beam; in such a case, the (orthogonal) pressure on a parallel wall is simply zero. In our approach this problem is avoided.

Section II gives, for the sake of readability, a brief account of the theoretical background in the linear case although this material is strictly speaking not new. In particular, we review how the equation of force equilibrium is solved when the input laser intensity is Gaussian. Section III then introduces our step-index fiber model. We use this model, as we indicated, to show how the balance of hydrodynamical and radiation forces leads to a stable equilibrium radius for a given power P in the laser beam. Comparison with the giant deformations observed in the Bordeaux experiments shows reasonably good agreement.

II. THEORETICAL BACKGROUND, LINEAR THEORY

The electromagnetic force density $\mathbf{f}$ in an isotropic, nonconductive, and nonmagnetic medium (see, for instance, Refs. [5,29]), is

$$\mathbf{f} = -\frac{\epsilon_0}{2}E^2\nabla n^2 + \frac{\epsilon_0}{2}\left[E^2\rho\left(\frac{\partial n^2}{\partial\rho}\right)_T\right] + \frac{n^2-1}{c^2}\frac{\partial}{\partial t}(\mathbf{E}\times\mathbf{H}). \tag{1}$$

We employ Système International (SI) units so that the relation $\epsilon_0\mu_0 = 1/c^2$ refers to a vacuum, and let ϵ be a relative quantity so that the constitutive relations are $\mathbf{D} = \epsilon_0\epsilon\mathbf{E}$, $\mathbf{B} = \mu_0\mathbf{H}$. The medium is assumed to be nondispersive. Only the first term in Eq. (1) contributes in our case; as mentioned above this is the Abraham-Minkowski (AM) force

$$\mathbf{f}^{\mathrm{AM}} = -\frac{\epsilon_0}{2}E^2\nabla n^2. \tag{2}$$

The geometry is sketched in Fig. 1 (we assume illumination of the surface from below). The incident wave is taken to be monochromatic, $\mathbf{E}^{(i)} = \mathbf{E}^{(i)}(\mathbf{r})e^{-i\omega t}$. The plane of incidence is

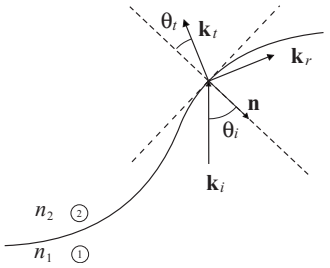

FIG. 1. Laser wave incident upon an interface separating media 1 and 2, where the index of refraction $n_1 < n_2$. The electromagnetic surface force is directed toward the optically thinner medium irrespective of the laser light's direction of propagation.

formed by the vectors $\mathbf{k}_i$ and $\mathbf{n}$; the angle of incidence is θ_i and the angle of transmission is θ_t (see Fig. 1). Let $\mathbf{E}_\parallel$ and $\mathbf{E}_\perp$ be the components of $\mathbf{E}$ parallel and perpendicular to the plane of incidence; then the respective transmission coefficients are

$$T_\parallel = \frac{\sin 2\theta_i \sin 2\theta_t}{\sin^2(\theta_i+\theta_t)\cos^2(\theta_i-\theta_t)}, \tag{3}$$

$$T_\perp = \frac{\sin 2\theta_i \sin 2\theta_t}{\sin^2(\theta_i+\theta_t)}. \tag{4}$$

Let $I = \epsilon_0 n_1 c\langle E^{(i)2}\rangle$ (averaged over the two polarizations) be the intensity of the incident beam. If α is the angle between $\mathbf{E}^{(i)}$ and the plane of incidence, so that $E_\parallel^{(i)} = E^{(i)}\cos\alpha, E_\perp^{(i)} = E^{(i)}\sin\alpha$, we can write the surface pressure as [27,28]

$$\mathbf{\Pi}^{AM} = -\frac{I}{2c}\frac{n_2^2-n_1^2}{n_2}\frac{\cos\theta_i}{\cos\theta_t}[(\sin^2\theta_i+\cos^2\theta_t)T_\parallel\cos^2\alpha + T_\perp\sin^2\alpha]\mathbf{n}. \tag{5}$$

Now let the liquid-liquid interface be represented as $z = h(r,\theta)$ in cylindrical coordinates ($r = \sqrt{x^2+y^2}$) and assume azimuthal symmetry, so that $h_\theta \equiv \partial h/\partial\theta = 0$. Observing that $\cos\theta_i = (1+h_r^2)^{-1/2}$, $\sin\theta_i = h_r(1+h_r^2)^{-1/2}$ ($h_r \equiv \partial h/\partial r$) as well as the corresponding relations for θ_t we obtain, upon substitution into Eq. (5),

$$\Pi = \frac{2n_1 I}{c}\frac{1-N}{1+N}f(h_r,\alpha), \tag{6}$$

where

$$N = n_1/n_2 < 1$$

is the refractive index ratio and $f(h_r,\alpha)$ is the function

$$f(h_r,\alpha) = \frac{(1+N)^2}{[N+\sqrt{1+h_r^2(1-N^2)}]^2}\left\{\sin^2\alpha + \frac{1+(3-N^2)h_r^2+(2-N^2)h_r^4}{[Nh_r^2+\sqrt{1+h_r^2(1-N^2)}]^2}\cos^2\alpha\right\}. \tag{7}$$

Now it turns out that the polarization plays no important part in the present problem. This can be seen by plotting the normalized radiation force for different values of the angle α (not shown here; some more details can be found in Refs.

[28,31]). Taking $N=0.986$, a physically realistic value in the Bordeaux experiments, it is hard even to separate the curves for varying values for α. In the actual experiments the values of N were indeed near unity. This gives an expression for $f(h_r,\alpha)\rightarrow f(N,h_r)$, averaged over the angle α, that is more than accurate enough for our purpose:

$$f(N,h_r)=(1+N^2)\frac{1+(2-N^2)h_r^2+h_r^4+Nh_r^2S}{(N+S)^2(Nh_r^2+S)^2}, \tag{8}$$

where $S\equiv\sqrt{1+h_r^2(1-N^2)}$.

The system that we shall consider is comprised of two near-critical oil-emulsions separated by an interface, caused by the density contrast between the liquids. It is useful to introduce the Bond number, describing the relative strength of buoyancy in comparison to the Laplace force:

$$B=\left(\frac{\omega_0}{l_C}\right)^2. \tag{9}$$

Here ω_0 is the radius of the beam waist, and l_C is the capillary length,

$$l_C=\sqrt{\frac{\sigma}{(\rho_1-\rho_2)g}}, \tag{10}$$

where σ is the surface tension, ρ_1 and ρ_2 are the densities of the lower and upper liquids, and g is the gravitational acceleration. In the experiments of Casner and Delville, the Bond numbers were in the range from 10^{-3} to about 4. If $B\ll 1$, the gravitational force is much weaker than the surface-tension force.

An advantage of near-critical systems is the possibility to tune fluid properties continuously by varying the temperature. Many physical quantities scale with temperature as $\propto[(T-T_C)/T_C]^{\beta}$, where β is a constant (see, for instance, [30]). Detailed information about liquid properties near to the critical point is available elsewhere [23,24,27,28] and will not be repeated here.

Consider now the governing equation for the liquid-liquid surface elevation. Under stationary conditions the elevation is determined by the balance of radiation pressure, surface tension, and gravity. Applying Laplace's formula for the pressure difference p_2-p_1, we obtain [27,28]

$$\Delta\rho g h(r)-\frac{\sigma}{r}\frac{d}{dr}\left[\frac{rh_r}{\sqrt{1+h_r^2}}\right]=-\frac{2I(r)}{c}n_1\frac{n_2-n_1}{n_2+n_1}f(N,h_r), \tag{11}$$

where $\Delta\rho=\rho_1-\rho_2>0$. The equation can be solved numerically once $I(r)$ is known.

Let us assume a Gaussian form:

$$I(r)=\frac{2P}{\pi\omega_0^2}e^{-2r^2/\omega_0^2}, \tag{12}$$

where P is the total power. It is convenient to introduce the dimensionless variables $R=r/\omega_0$, $H(R)=h(r)/\omega_0$, whereby Eq. (11) can be written in dimensionless form:

$$BH-\frac{1}{R}\frac{d}{dR}\left[\frac{RH_R}{\sqrt{1+H_R^2}}\right]=-Fe^{-2R^2}f(N,H_R), \tag{13}$$

with

$$F\approx\frac{2P|\partial n/\partial\rho|}{\pi c g\omega_0 l_C^2}. \tag{14}$$

The function $f(N,H_R)$ is the same as given by Eq. (8) above, except from the replacement $h_r\rightarrow H_R$. As before, $B=(\omega_0/l_C)^2$ is the Bond number, and $|\partial n/\partial\rho|=1.22\times10^{-4}$ m^3/kg [21]. The ratio N, and the capillary length l_C, are the only temperature-dependent parameters. Thus there are three parameters in Eq. (13), namely, the temperature difference ΔT, the beam waist ω_0, and the beam power P.

Numerical solutions of Eq. (13) are shown in Fig. 2. Similar results are presented in Ref. [28], except that in the present case the theoretical curve is compared directly with experimental data from the Bordeaux group. Profiles of the deformations are extracted from images taken by a charge-coupled device (CCD) camera [provided by Jean-Pierre Delville (personal communication)]. As is seen, the numerical solution gives excellent results for a laser power of $P=450$ mW, beam waist $\omega_0=5.3$ μm, and $\Delta T=T-T_C=3.5$ K. If the laser power is increased, the correspondence between theory and experiment becomes poorer. For instance, insertion of the large power $P=1200$ mW in the formulas would lead to a considerable overprediction (about 50%) of the surface displacement. This concludes our overview of the linear theory.

III. ELECTROMAGNETIC WAVE ANALYSIS

When the power of the laser is increased (for a fixed beam width) beyond a certain threshold, the behavior of the liquid-liquid interface deformation becomes nonlinear. It has been observed that a "shoulder" appears in the case where light propagates in the upward direction (cf., for instance, Ref. [21]). If the light propagates downward, the deformations become very large and cylinderlike, eventually forming a jet. The deformations may even form a liquid bridge crossing a central layer of fluid. In such a case it is natural to suggest that the deformations, or rather the liquid column, may be regarded as an *optical fiber*, capable of guiding the laser-light due to internal reflections. As already mentioned, this is the main idea of the present paper. Furthermore, the deformations and columns tend to have vertical walls, which corresponds to $|h_r|\rightarrow\infty$.

Examining the expression (6) for the radiation pressure, it can be seen that (see Fig. 3)

$$\Pi^{AM}\rightarrow 0 \quad \text{when } |h_r|\rightarrow\infty,$$

implying that the radiation force vanishes, leaving only the forces of surface tension and gravity, which both act against any deformation of the interface. This result is obviously unphysical, since both steep-walled deformations, and the liquid columns, are stationary structures. This means that the following two usual assumptions:

(i) the laser-beam intensity distribution is Gaussian, and stays Gaussian also in the region being deformed; and

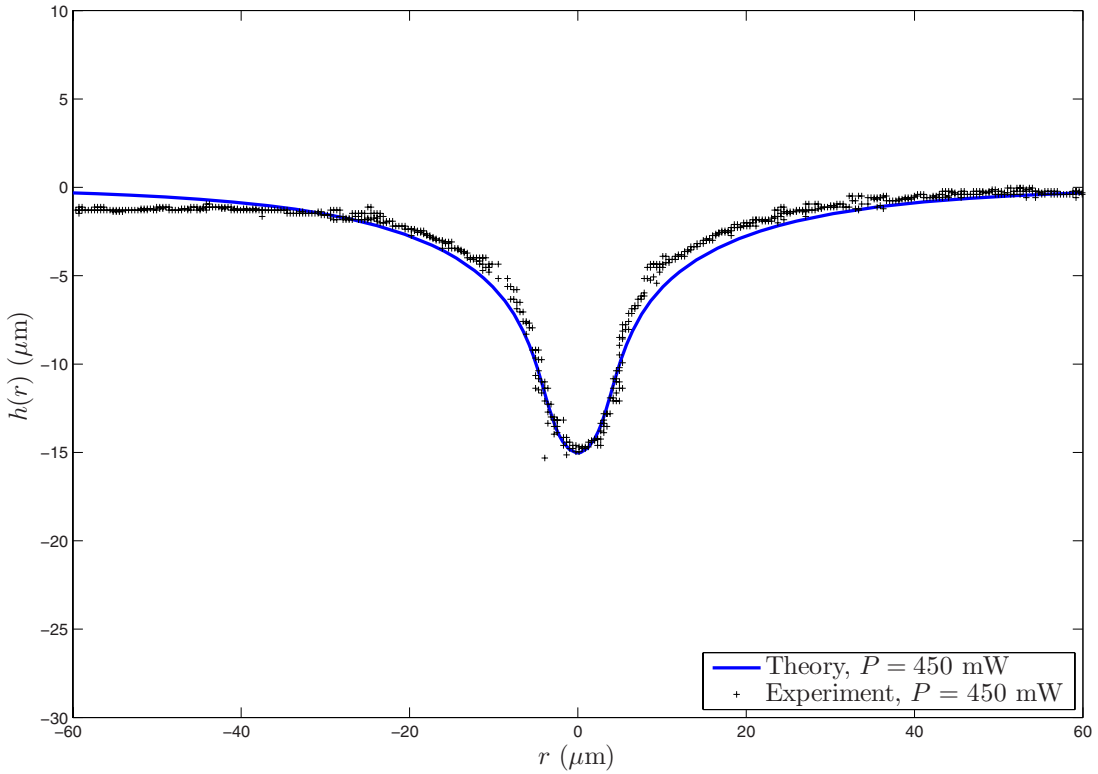

FIG. 2. (Color online) Experimental versus numerical results at temperature such that $\Delta T = T - T_C = 3.5$ K, and with a laser beam waist of $\omega_0 = 5.3$ μm at a power of 450 mW.

(ii) ray optics may be used to describe the path of a light beam within the deformation, must be invalid. Regarding the intensity distribution, one can argue that the geometrical change of the illuminated interface will result in new boundary conditions that the electromagnetic field must satisfy. In turn, this gives rise to a different, and unknown, intensity distribution within the huge deformations characteristic of the nonlinear regime. Also, ray-optics may give a poor description of the propagation of the electromagnetic waves within the structure. In our optical fiber model the core of radius $r=a$ is the upper liquid, and the cladding is the surrounding liquid (the lower liquid). Solving Maxwell's equations for such a geometry, and relating the power flow through the structure to the power of the incident laser beam, one should be able to obtain a more reliable expression for the radiation pressure, and give an estimate for its magnitude.

A. Derivation of the modified radiation force

Assume as before plane-wave propagation and sinusoidal time-dependence of the fields, $E, B \propto e^{-i\omega t}$. Maxwell's equations may be combined to give the following Helmholtz wave equations for $\mathbf{H}$ and $\mathbf{E}$ (cf., for instance, Ref. [32]):

$$\nabla^2 \mathbf{H} + \frac{n^2\omega^2}{c^2}\mathbf{H} = i\omega\epsilon_0(\nabla n^2) \times \mathbf{E}, \tag{15}$$

$$\nabla^2 \mathbf{E} + \frac{n^2\omega^2}{c^2}\mathbf{E} = -\nabla\left[\frac{1}{n^2}(\nabla n^2)\cdot\mathbf{E}\right]. \tag{16}$$

By taking the z components of Eqs. (15) and (16), and eliminating the transverse field components, one finds the two-dimensional scalar wave equations for the system,

$$\nabla_t^2 H_z + \gamma^2 H_z - \left(\frac{\omega}{\gamma c}\right)^2 (\nabla_t n^2)\nabla_t H_z = -\frac{\omega k_z \epsilon_0}{\gamma^2}\hat{\mathbf{z}}\cdot[\nabla_t n^2 \times \nabla_t E_z], \tag{17}$$

and

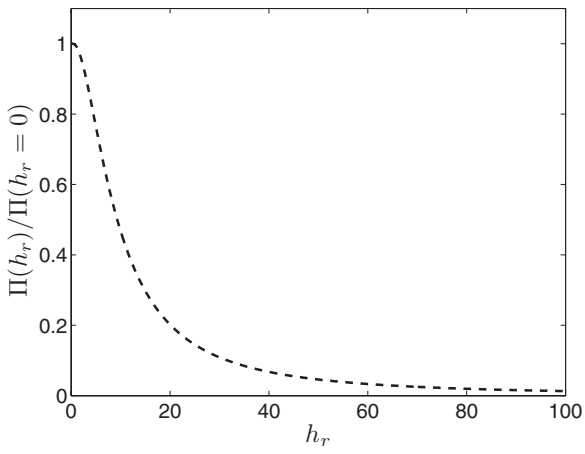

FIG. 3. The function $f(N, h_r)$ goes to zero as h_r grows large, i.e., when the walls of the deformation, or the liquid column, are (nearly) vertical. The only remaining forces are then the Laplace force and the hydrostatic pressure force, both acting inward. This implies that the column or deformation should collapse in on itself, which it evidently does not.

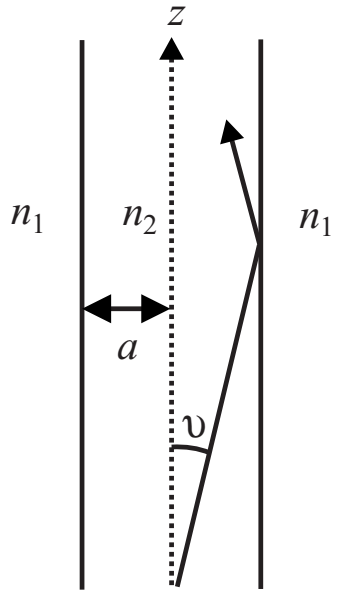

FIG. 4. Section of the deformation modeled as an optical step-index fiber.

$$\nabla_t^2 E_z + \gamma^2 H_z - \left(\frac{k_z}{\gamma n}\right)^2 (\nabla_t n^2)\nabla_t E_z = \frac{\omega k_z \mu_0}{\gamma^2 n^2}\hat{\mathbf{z}} \cdot [\nabla_t n^2 \times \nabla_t H_z]. \tag{18}$$

where $\nabla_t^2 = \nabla^2 - \partial_z^2$ is the transverse part of the Laplacian operator. The solutions to these equations are

$$\{E_z, H_z\} = \{A_e, A_h\} J_m(\gamma r) e^{im\theta + ik_z z - i\omega t}, \quad r < a \tag{19}$$

and

$$\{E_z, H_z\} = \{B_e, B_h\} K_m(\beta r) e^{im\theta + ik_z z - i\omega t}, \quad r > a. \tag{20}$$

Here, m is an integer, J_m is the mth Bessel function of the first kind, and K_m is a modified Bessel function. The radius of the deformation (the core radius) is $r=a$. The constants A_e, A_h, B_e, and B_h are determined from the boundary conditions at $r=a$. Furthermore,

$$\gamma^2 = \omega^2 n_2^2/c^2 - k_z^2 = k_0^2 n_2^2 - k_z^2 \equiv k_2^2 - k_z^2 \quad (r < a),$$

$$\beta^2 = k_z^2 - \omega^2 n_1^2/c^2 = k_z^2 - k_0^2 n_1^2 \equiv k_z^2 - k_1^2 \quad (r > a)$$

are the radial propagation constants. k_z is the longitudinal wave number, given by $k_z = k_2 \cos\vartheta$, with ϑ being the angle of propagation. See Fig. 4. Note that $k_0 = \omega/c$ refers to the vacuum, $k_2 = k_0 n_2$ refers to the core, and $k_1 = k_0 n_1$ refers to the cladding.

Inserting the solutions (19) and (20) into the wave equations (17) and (18), one can find the radial and azimuthal field components. Detailed calculations are given in the books of Stratton [29] and Okamoto [33]. One has to observe that there are multiple solutions to Maxwell's equations for the step-index geometry, corresponding to different modes of propagation. We restrict ourselves here to giving the expressions for the radial and azimuthal components for the electric field inside the fiber, $r<a$,

$$E_r = \left\{ i\frac{k_z A_e}{\gamma} J_m'(\gamma r) - \frac{\omega \mu_0 m A_h}{\gamma^2 r} J_m(\gamma r) \right\} e^{im\theta + ik_z z - i\omega t},$$

$$E_\theta = -\left\{ \frac{k_z m A_e}{\gamma^2 r} J_m(\gamma r) + i\frac{\omega \mu_0 A_h}{\gamma} J_m'(\gamma r) \right\} e^{im\theta + ik_z z - i\omega t},$$

$$E_z = A_e J_m(\gamma r) e^{im\theta + ik_z z - i\omega t}, \tag{21}$$

and similarly the H field for $r<a$,

$$H_r = \left\{ i\frac{k_z A_h}{\gamma} J_m'(\gamma r) + \frac{\omega \epsilon_0 n_2^2 m A_e}{\gamma^2 r} J_m(\gamma r) \right\} e^{im\theta + ik_z z - i\omega t},$$

$$H_\theta = \left\{ -\frac{k_z m A_h}{\gamma^2 r} J_m(\gamma r) + i\frac{\omega \epsilon_0 n_2^2 A_e}{\gamma} J_m'(\gamma r) \right\} e^{im\theta + ik_z z - i\omega t},$$

$$H_z = A_h J_m(\gamma r) e^{im\theta + ik_z z - i\omega t}. \tag{22}$$

The prime on the Bessel functions indicates differentiation with respect to the argument γr.

The aim now is to determine the allowed discrete angles ϑ at which the light rays may propagate, corresponding to the allowed modes of propagation. We begin by defining the normalized transverse wave numbers as

$$u \equiv \gamma a = a\sqrt{k_2^2 - k_z^2}, \tag{23}$$

$$w \equiv \beta a = a\sqrt{k_z^2 - k_1^2}. \tag{24}$$

Furthermore, the wave numbers u and w are related, from Eq. (36), as

$$u^2 + w^2 = k_0^2(n_2^2 - n_1^2)a^2 \equiv v^2, \tag{25}$$

referred to as the *normalized frequency*. The boundary conditions are that the tangential field components are continuous across $r=a$. From them the general dispersion relation is constructed, valid for all values of $N = n_1/n_2 < 1$ [33]:

$$\left[\frac{J_m'(u)}{uJ_m(u)} + \frac{K_m'(w)}{wK_m(w)}\right]\left[\frac{J_m'(u)}{uJ_m(u)} + N^2\frac{K_m'(w)}{wK_m(w)}\right] = m^2\left(\frac{1}{u^2} + \frac{1}{w^2}\right)\left[\frac{1}{u^2} + \frac{N^2}{w^2}\right]. \tag{26}$$

B. Fundamental mode of the step-index fiber: Calculation of the equilibrium radius

To simplify the discussion, we shall from now on consider only the fundamental mode of the step-index optical fiber. This mode corresponds to the $m=1$ solution of the scalar wave equation and is called a hybrid mode. The fundamental mode of a step-index optical fiber is the $HE_{m=1,l=1}$ mode, corresponding to both E_z and H_z nonzero [33,34], in contrast to the transverse electric (TE) and transverse magnetic (TM) modes which correspond to $m=0$ having E_z and H_z equal to zero, respectively, but which possess low cutoff frequencies.

The index $l=1$ corresponds to the first root of the dispersion relation satisfying $k_1 < k_z < k_2$. The HE_{11} mode has no

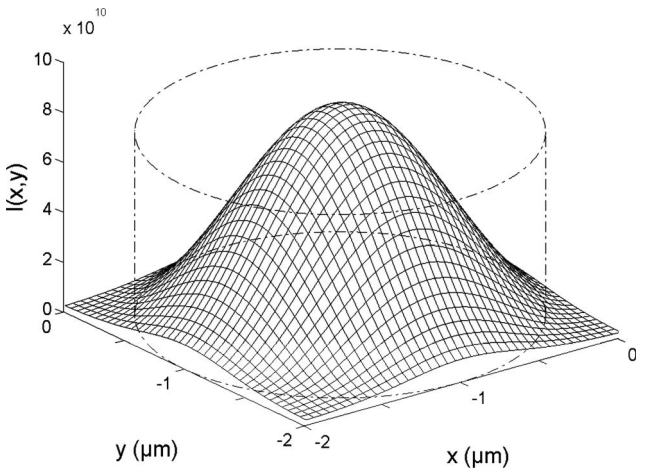

FIG. 5. The intensity distribution for the HE_{11} mode in a step-index fiber of radius $a=2$ μm, at a laser beam power of 500 mW, and with $\Delta T=3.5$ K. Broken lines indicate the fiber boundary.

cutoff frequency; this is the reason why it is regarded as the fundamental mode of a step-index fiber. For a typical fiber in optics, the relative refractive index difference $\Delta=1-n_1/n_2$ is on the order of 0.01. This suits well with the conditions of the Bordeaux experiments: with the typical value of $N=0.986$ as mentioned above, we get $\Delta=0.014$, which is quite appropriate. Under such conditions the confinement of light in the core is not so tight (this is called the weakly guiding approximation). The approximation $N\approx 1$ allows one to simplify the theory of optical fibers very much and to obtain clear-cut results. The accuracy of adopting the HE_{11} mode as a basis in our model should be more than sufficient.

A sketch of the intensity distribution for this mode is given in Fig. 5. Numerically solving the dispersion relation (26) for a given fiber radius a, we obtain the wave number k_z corresponding to that particular radius. Repeating this procedure for a range of radii, and with all field components being known, we can calculate the components of the Abraham-Minkowski surface force density on the interface of a fiber with a given diameter. The expression for the AM surface pressure reads

$$\mathbf{\Pi}^{AM}=\frac{\epsilon_0}{2}(n_2^2-n_1^2)[E_\theta^2+E_z^2+N^{-2}E_r^2]_{r=a-}\mathbf{n}. \tag{27}$$

Here

$$\mathbf{n}=(1+h_x^2+h_y^2)^{-1/2}(h_x,h_y,-1) \tag{28}$$

is the normal vector to the interface, pointing from the internal medium 2 to the external medium 1. If $\mathbf{S}=\frac{1}{2}(\mathbf{E}\times\mathbf{H}^*)$ denotes the Poynting vector, the total power P carried by the optical fiber plus the cladding is given by

$$P=\int_0^{2\pi}\int_0^\infty S_z r dr d\theta=\frac{1}{2}\int_0^{2\pi}\int_0^\infty (E_r H_\theta^*-E_\theta H_r^*)r dr d\theta. \tag{29}$$

Some calculation yields

$$P=P_{\text{core}}+P_{\text{clad}}=\frac{\pi}{4}\epsilon_0 c a^2|A|^2\left[n_2F(J_0,J_1)+n_1\frac{J_1^2}{K_1^2}G(K_0,K_1)\right], \tag{30}$$

where

$$F(J_0,J_1)\equiv\frac{k_z^2a^2}{u^2}\left[(1+s^2)(J_0^2+J_1^2)-\frac{2}{u^2}(1+s)^2J_1^2\right]+J_0^2+J_1^2-\frac{2J_0J_1}{u}, \tag{31}$$

and

$$G(K_0,K_1)\equiv\frac{k_z^2a^2}{w^2}\left[(1+s^2)(K_1^2-K_0^2)+\frac{2}{w^2}(1+s)^2K_1^2\right]+\frac{2}{w}K_0K_1. \tag{32}$$

Here, it is understood that $J_n,K_n=J_n(u),K_n(u)$. The constant A is equal to A_e above, and B_e has been eliminated via the boundary condition $E_z(a-)=E_z(a+)$. The parameter s is given by

$$s\equiv\frac{\left(\frac{1}{u^2}+\frac{1}{w^2}\right)}{\left[\frac{J_1'(u)}{uJ_1(u)}+\frac{K_1'(w)}{wK_1(w)}\right]}\approx -1 \tag{33}$$

(cf. Ref. [33]). When the steepness is large ($h_r\gg 1$) the expression for the Laplace force in the radial direction takes on the simple form

$$f_L=-\lim_{h_r\to\infty}\frac{\sigma}{r}\frac{d}{dr}\frac{rh_r}{\sqrt{1+h_r^2}}=-\frac{\sigma}{r}. \tag{34}$$

The force balance may then be written as

$$-\Delta\rho g h(r=a)+\frac{\sigma}{a}=\Pi^{AM}(r=a). \tag{35}$$

This equation can be interpreted physically: The right-hand side is the AM surface force density acting outward. It is positive because $n_2>n_1$. This force is balanced by the Laplace force σ/a acting inward, plus the net hydrostatic pressure $-\Delta\rho g h(r=a)=-(\rho_1-\rho_2)gh(r=a)$, which also acts inwards because $\rho_1>\rho_2$. Notice that $h(r)$ is a negative quantity. We do not regard a as a fixed parameter, but rather determine the magnitude of the radiation pressure for a range of given values of a, and subsequently find the corresponding equilibrium radii where the radiation pressure exactly balances the forces of surface tension and hydrostatic pressure. Ergo, the thickness of the liquid column will vary with depth. For a given depth, the hydrostatic pressure difference is known, and then it is easy to determine the new equilibrium radius a. Notice that we still regard the structure as an ideal step-index fiber, although in fact it is not. The fiber rather resembles a tapered cylinder, which would require a different solution to Maxwell's equations to get exact results; but in our model, it seems reasonable to regard the fiber

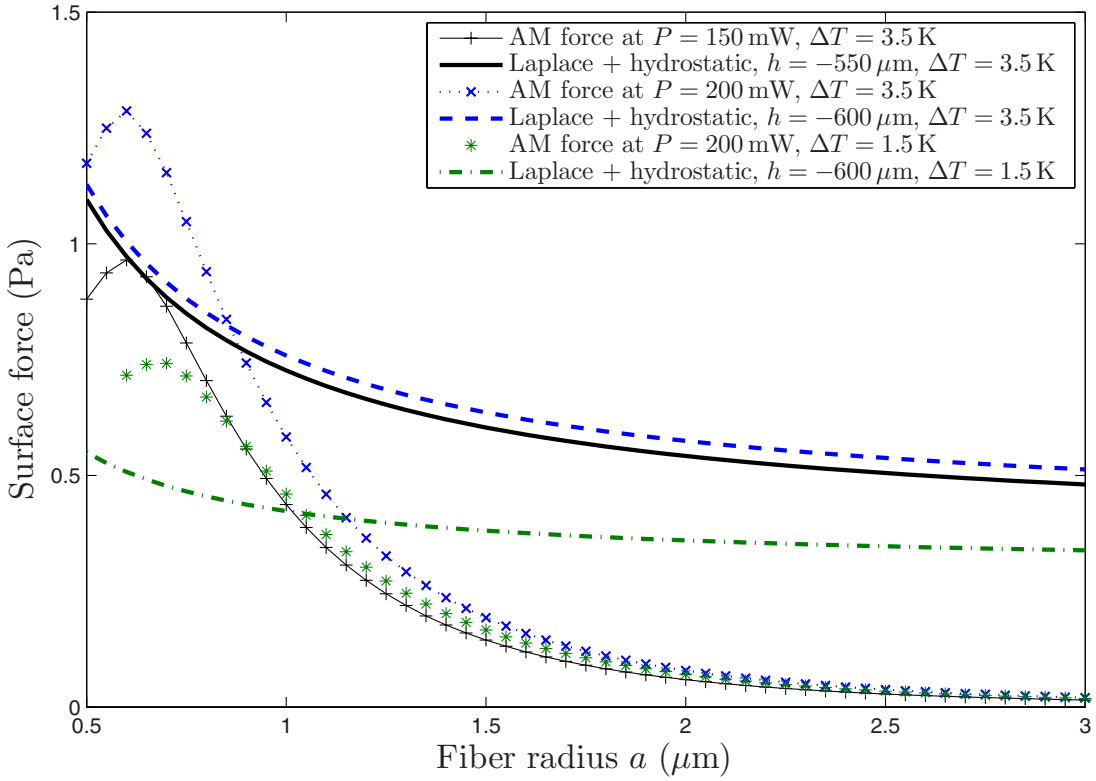

FIG. 6. (Color online) The electromagnetic radiation pressure (AM force) plotted as a function of varying fiber radius a, at given temperature ΔT and beam power P.

locally (with depth) as an optical cylindrical guide with zero taper.

Figure 6 shows how the electromagnetic radiation AM force varies versus the fiber radius a, for given values of ΔT and P. The combined pressure of surface tension (the Laplace force) and gravity (hydrostatic pressure) is also plotted. Intersect points correspond to equilibrium radii. Notice the middle set of curves with power $P=150$ mW. Here, the termination point of the liquid column can clearly be seen. As the depth increases beyond 550 μm, the outward acting AM force can no longer support the liquid column due to increasing hydrostatic pressure and surface tension. The model therefore predicts that at these parameter values, the liquid column can maximally reach a depth of $\sim$500 μm before collapsing, in good correspondence with observed breakups of the liquid columns into droplet spraying jets at depths of around 1000 μm. In our simple model we do not take into account the fluid flow inside the column; nevertheless, the model offers a simple and intuitive explanation of the observed pinch off of the columns.

With increasing temperature difference ΔT the radiation force becomes weaker relative to the Laplace force and the hydrostatic pressure (details not shown here). This behavior is expected, since the surface tension is temperature dependent and an increase in ΔT leads to a higher surface tension. Now the hydrostatic pressure slightly increases as the density contrast increases, but this is not of great importance since the term $\Delta\rho g h$ is very small. The net behavior is that for higher ΔT the equilibrium radii become smaller.

In Fig. 7, the two left panels refer to temperature differences, $\Delta T=\{3.5, 1.5\}$ K, and to a moderate power, $P=200$ mW. These parameter values make our model quite justifiable, as can be seen from the following argument.

(1) When ΔT is small the relative refractive index becomes also small, in our case amounting to 0.55% (i.e., $\Delta = 1-n_1/n_2=0.0055$). The microemulsion liquid used in the Bordeaux experiments had a temperature-dependent refractive index of around 1.46 ([21]). The laser used was an argon laser operating in the TEM_{00} mode, with a vacuum wavelength of $\lambda_0=0.514$ μm. From these values we calculate the normalized frequency

$$v = k_0 a \sqrt{n_2^2 - n_1^2} = 1.88a\ [\mu\mathrm{m}]. \tag{36}$$

(2) The second point is that for moderate powers the equilibrium radii for the liquid column become small. Physically, the reason is that the AM outward pressure is not strong enough to widen the column very much. The two left panels in Fig. 7 show that for $P=200$ mW the radii are about 1 μm. It is instructive here to compare with Fig. 3 in Okamoto's book [33], which shows the occurrences of multiple modes in a typical single-step fiber. As long as v is less than about 2.4, only the basic HE_{11} mode appears. For increasing v, up to 3.5, perhaps even higher, there occurs a mixture with the next HE_{21} mode, but we find it reasonable to expect that the basic mode is the dominant one at least up to about $v=3$. Insertion of $a=1$ μm in Eq. (36) yields $v\approx 2$. Accordingly, the single-mode model ought in this case to be a viable one. Also, we note from Fig. 7 that the *uniform-cylinder* model of the column turns out to be a good approximation, as the slope of the column is large, $|h_r| \sim 10^4$.

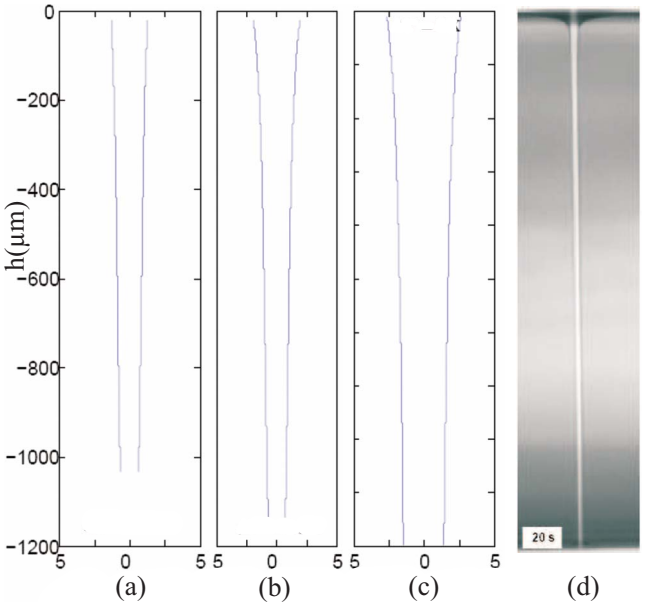

FIG. 7. (Color online) Calculated interface deformation resulting from the balance between the modified AM force, the Laplace force, and the hydrostatic force. (a) and (b) $P=200$, and $\Delta T=\{3.5,1.5\}$ K, respectively. At this moderate power level and values of ΔT, the radii of the columns are, according to the model, around 1 μm, thus satisfying the single-mode condition of the step-index fiber. At high power $P=1750$ mW and $\Delta T=6$ K, shown in (c), the column is predicted to be slightly wider with a radius from 1.5 to 3 μm. (d) Taken from Ref. [21], it shows the liquid column resulting from illuminating the surface from above with a laser at $P=1750$ mW, and with $T-T_C=6$ K. In Ref. [21] it is stated that the jet is about 1000 μm deep, with a radius around 7 μm, i.e., of the same order of magnitude as that calculated in our model.

Actually, it seems that the above limits for the applicability of the single-mode model may be stretched considerably. The third panel of Fig. 7 shows the predicted column width when the power is high, $P=1750$ mW. This is in violation of the single-mode condition, but still the calculated results yield a figure visually quite similar to the experimental deformation shown in the rightmost frame. The last-mentioned frame, taken from Ref. [21], shows a long jet with large radius, $a\approx 7$ μm. The good agreement between theory and experiment indicates that the single-step model is quite robust.

The last point that we shall focus attention on is the observed termination, or "pinch off," of the liquid column at large depths where the radius becomes small. We can obtain a semiquantitative explanation of this effect on the basis of our model. Namely, when a becomes smaller than about 0.6 μm the repulsive AM radiation force is no longer able to withstand the inward directed Laplace and hydrostatic forces (there is no equilibrium point in Fig. 6) and the column has to collapse. What one actually observes in experiments is that the column breaks up into a row of small droplets. In Figs. 7(a) and 7(b), the theoretical pinch off of the columns is seen to occur at depths of around 1000 μm. At equal power, the column stretches deeper when the surface tension is lower ($\Delta T=1.5$ K). It is, moreover, observed that the breakup occurs in the case of illumination from above only. Our model is, however, unable to explain that particular effect. No theory for it seems to be known.

IV. SUMMARY

Let us summarize our work as follows.

(1) Our main idea has been to model the large fingerlike deformations, the liquid columns and liquid jets seen in laser optics experiments, as optical waveguides or fibers. We have identified the electric field components of a step-index fiber, identifying the HE_{11} mode as the fundamental mode. The HE_{11} mode is a hybrid mode, thus more complicated than the conventional TE and TM modes in that the axial electromagnetic fields E_z and H_z are not zero, but it is precisely this mode that is the dominant one in conventional step-index fibers when the index contrast $N=n_1/n_2$ is close to 1 [33]. The fact that the giant deformations are seen experimentally in the vicinity of the critical point when $N\approx 1$ makes our fiber model very natural from a physical viewpoint. Moreover, the experiments performed by the Bordeaux group [21,3,22–26] correspond just to $N\approx 1$.

(2) In Sec. II we reviewed the linear theory, showing how the elevation of the interface can be calculated with quite good accuracy for low laser powers P when comparing with the Bordeaux experiments. No attempt was, however, made to calculate the elevations in the nonlinear, high-power case. In particular, we did not consider the formation of a "shoulder" as seen experimentally upon illumination from below. No theory for the nonlinear case seems so far to exist. Instead, we made use of our model to show how the balance between hydrodynamical and radiation forces leads to the establishment of stable radii for the liquid column. See Fig. 6. This means that a physical explanation is given for the establishment of these giant structures. We emphasize that such a result is not obtainable from conventional radiation theory assuming a Gaussian intensity profile for the incident laser beam. Our intensity distribution described by the HE_{11} mode is different from the Gaussian form. See the more detailed discussion on this point in the first part of Sec. III.

(3) Our comparisons with experiments are all made with reference to the Bordeaux group. Figure 7 shows how our calculated values for the column radius a correspond quite well with the values observed. In particular, the narrowing of the width for increasing depths is reproduced. Such a narrowing, by a factor of 2 or more, is typically seen in experiments [Jean-Pierre Delville (personal communication)].

Note added. Recently, we became aware of two papers by the Bordeaux group [35,36]. These papers report on both theoretical and experimental work. As for the theoretical parts, they are closely related to our above approach.

ACKNOWLEDGMENT

We thank Jean-Pierre Delville for valuable information about the recent Bordeaux experiments.

[1] J. H. Poynting, Philos. Mag. **9**, 393 (1905).
[2] A. Ashkin and J. M. Dziedzic, Phys. Rev. Lett. **30**, 139 (1973).
[3] R. D. Schroll, R. Wunenburger, A. Casner, W. W. Zhang, and J. P. Delville, Phys. Rev. Lett. **98**, 133601 (2007).
[4] C. Møller, *The Theory of Relativity*, 2nd ed. (Clarendon, Oxford, 1972), Sec. 7.7.
[5] I. Brevik, Phys. Rep. **52**, 133 (1979); cf. also I. Brevik, Phys. Rev. B **33**, 1058 (1986).
[6] G. W. Kentwell and D. A. Jones, Phys. Rep. **145**, 319 (1987).
[7] S. Antoci and L. Mihich, Eur. Phys. J. D **3**, 205 (1998).
[8] Y. N. Obukhov and F. W. Hehl, Phys. Lett. A **311**, 277 (2003).
[9] R. Loudon, L. Allen, and D. F. Nelson, Phys. Rev. E **55**, 1071 (1997).
[10] J. C. Garrison and R. Y. Chiao, Phys. Rev. A **70**, 053826 (2004).
[11] A. Feigel, Phys. Rev. Lett. **92**, 020404 (2004).
[12] U. Leonhardt, Phys. Rev. A **73**, 032108 (2006).
[13] O. J. Birkeland and I. Brevik, Phys. Rev. E **76**, 066605 (2007).
[14] A. Ashkin, J. M. Dziedzic, J. E. Bjorkholm, and S. Chu, Opt. Lett. **11**, 288 (1986).
[15] G. I. Taylor, Proc. R. Soc. London, Ser. A **313**, 453 (1969).
[16] R. Badie and D. Frits de Lange, Proc. R. Soc. London, Ser. A **453**, 2573 (1997).
[17] A. M. Gañan-Calvo, J. Dávila, and A. Barrero, J. Aerosol Sci. **28**, 249 (1997).
[18] L. Oddershede and S. R. Nagel, Phys. Rev. Lett. **85**, 1234 (2000).
[19] E. Schäffer, T. Thurn-Albrecht, T. P. Russell, and U. Steiner, Nature (London) **403**, 874 (2000).
[20] H. L. Rosano and M. Clausse, *Microemulsion Systems*, Surfactant Science Series (Dekker, New York, 1987).
[21] A. Casner, Ph.D. thesis, Université Bordeaux I, Bordeaux, France, 2002; http://tel.archives-ouvertes. fr/tel-00001637.
[22] A. Casner and J. P. Delville, Opt. Lett. **26**, 1418 (2001).
[23] A. Casner and J. P. Delville, Phys. Rev. Lett. **87**, 054503 (2001).
[24] A. Casner and J. P. Delville, Phys. Rev. Lett. **90**, 144503 (2003).
[25] R. Wunenburger, A. Casner, and J. P. Delville, Phys. Rev. E **73**, 036314 (2006).
[26] R. Wunenburger, A. Casner, and J. P. Delville, Phys. Rev. E **73**, 036315 (2006).
[27] J. P. Delville, A. Casner, R. Wunenburger, and I. Brevik, *Trends in Electro-Optics Research* (Nova Science, New York, 2006), pp. 1–58.
[28] A. Hallanger, I. Brevik, S. Haaland, and R. Sollie, Phys. Rev. E **71**, 056601 (2005).
[29] J. A. Stratton, *Electromagnetic Theory* (McGraw-Hill, New York, 1941).
[30] E. Freysz, M. Afifi, and A. Ducasse, J. Phys. (France) Lett. **46**, L181 (1985).
[31] O. J. Birkeland and I. Brevik, e-print arXiv:0802.0575v1.
[32] J. D. Jackson, *Classical Electrodynamics*, 3rd ed. (Wiley, New York, 1999), Sec. 8.11.
[33] K. Okamoto, *Fundamentals of Optical Waveguides*, 2nd ed. (Elsevier, Amsterdam, 2006).
[34] E. Snitzer, J. Opt. Soc. Am. **51**, 491 (1961).
[35] E. Brasselet, R. Wunenburger, and J. P. Delville, Phys. Rev. Lett. **101**, 014501 (2008).
[36] E. Brasselet and J. P. Delville, Phys. Rev. A **78**, 013835 (2008).